Available online at www.sciencedirect.com
SCIENCE DIRECT
Journal of the European Ceramic Society 26 (2006) 2619–2625
www.elsevier.com/locate/jeurceramsoc

Percolative mechanism of sliding wear in alumina/zirconia composites

José F. Bartolomé [a], Carlos Pecharromán [a], José S. Moya [a,*], Antonia Martín [b], José Ygnacio Pastor [b], Javier Llorca [b]

[a] *Instituto de Ciencia de Materiales de Madrid (ICMM), Consejo Superior de Investigaciones Científicas (CSIC), Cantoblanco, 28049 Madrid, Spain*
[b] *Departamento de Ciencia de Materiales, Universidad Politécnica de Madrid, C/Profesor Aranguren s/n, 28040 Madrid, Spain*

Received 6 March 2005; received in revised form 4 May 2005; accepted 15 May 2005
Available online 27 July 2005

Abstract

In the present study, the wear resistance of zirconia-toughened alumina (ZTA) composites has been investigated under dry sliding conditions with a Hertzian contact pressures from 1.1 up to 2.2 GPa and a sliding velocity of 0.15 m/s. The wear rate for composite with 22 vol.% zirconia (3Y-TZP) content at the lower contact pressures (1.1 GPa), was found to be around two orders of magnitude higher than the ones corresponding to 14 and 7 vol.% 3Y-TZP content. This result has been explained in terms of the infinite cluster formed at the percolation threshold. Above the critical 3Y-TZP fraction of ≈16 vol.%, corresponding to the percolation threshold, a continuous path between zirconia particles takes place. In these particular cases, the wear is dominated by a percolative mechanism so that the t → m zirconia transformation creates a microcracks network, which controls the wear resistance of the composite.

Keywords: Wear resistance; Phase transformation; Al_2O_3; ZTA

1. Introduction

Previous investigations showed the importance and benefit of the use of ZTA (zirconia-toughened alumina) for tribological purposes.[1–5] It was found that the transition from a mild to a severe wear process in these composites can be shifted to more extreme operating conditions, for instance, higher loads and higher velocities.[4,6,7] The use of metastable zirconia particles as a reinforcing element improves wear resistance through the suppression of crack initiation and propagation due to the higher value of fracture toughness. Moreover, it must be possible to inhibit the grain growth of the alumina phase during sintering, if a homogeneous distribution of the zirconia phase is obtained. Decreasing grain size results in an increasing in the wear transition load. However, zirconia has a disadvantage in its lower thermal conductivity ZrO_2 (1.85 W m^{-1} K^{-1}) than that of Al_2O_3 (30 W m^{-1} K^{-1}). In a tribological contact, frictional heating occurs and the low thermal conductivity induces thermal stresses at the subsurface layer by largely localized thermal gradients. Due to frictional heating, He et al.[8] have found, for a Hertzian contact pressure between 356 and 409 MPa with a maximum sliding speed of 0.09 m/s, a surface temperature about 800 °C and 200 °C for zirconia and Al_2O_3, respectively. Microfractures at the subsurface easily take place due to thermal stresses in combination with the mechanical stresses generated by the load, especially in the area of grain boundaries.[9] In this case, partial zirconia phase transformation can be induced either thermally or by mechanical stresses during sliding. The occurrence of a zirconia phase transformation prevents the formation of microcracks on the top surface, but weakens the grain boundaries at the subsurface layer because generates internal stresses that promote delamination and pullout, resulting in a decrease in wear resistance.[8,10–14]

* Corresponding author. Tel.: +34 91 334 9083; fax: +34 91 334 9083.
E-mail address: jsmoya@icmm.csic.es (J.S. Moya).

0955-2219/$ – see front matter © 2005 Elsevier Ltd. All rights reserved.
doi:10.1016/j.jeurceramsoc.2005.05.008

The aim of the present investigation is to study the sliding wear of ZTA composites with a Y-TZP content ranging from 7 to 22 vol.% in order to evaluate the effect of the infinite cluster formed at the percolation threshold on the wear resistance of ZTA composites.

2. Experimental procedure

2.1. Materials processing

A high purity alumina powder α-Al_2O_3 > 99.9 wt.% (Condea HPA 0.5, Ceralox division, Arizona, USA) with an average particle size of 0.49 μm and a specific surface area of 10 m^2/g (values given by the supplier) was mixed with 7, 14 and 22 vol.% of yttria-stabilised zirconia powder (3Y-TZP, Tosoh TZ-3YS, Tosoh Corp., Tokyo, Japan) with a mean particle diameter of 0.59 μm and a specific surface area of 6.7 m^2/g (values given by supplier). Stable aqueous suspensions of 70 wt.% solids content using 0.5 wt.% addition of an alkali-free organic polyelectrolite (Dolapix C64) were obtained. The suspensions were highly dispersed, exhibiting pseudo-plastic flow behaviour and low viscosity ($\tau \leq 10$ mPas at shear rate of 500 s^{-1}). Before carrying out the measurements, bubbles were removed by slow speed agitation. Ball milling was then performed using high purity alumina balls in an alumina jar for 24 h. Plates (100 mm × 100 mm × 5 mm) were cast from each suspension in plaster of Paris mould and dried in air at room temperature for 48 h. Samples were then sintered at 1600 °C for 2 h in air with heating and cooling rates of 300 °C/h. Sintered plates were then machined to small bars of 4 mm × 3 mm × 80 mm. The contact surfaces of the bars were polished down to 6 μm. The bulk density of >98% was determined for all sintered samples using the Archimedes technique in mercury.

2.2. Microstructural characterization

Scanning electron microscopy (SEM) micrographs were obtained using a Philips XL20 with an accelerating tension of 25 kV. Samples were cross-sectioned and polished with diamond paste down to 1 μm and subsequently thermally etched at 1450 °C in air for 30 min, with heating and cooling rates of 400 °C/h. Samples were then gold-coated before SEM analysis.

The grain size of the alumina matrix was determined using the linear intercept method[15] on SEM representative pictures.

2.3. Mechanical properties

The bending strength, σ_f, was determined by three-point bending test. The specimens were tested at room temperature using a three-point support with a span of 60 mm in a universal testing machine (Instron Model 4411). The specimens were loaded to failure with a cross-head speed of 0.005 cm/min. Reported strengths represented the mean and standard deviation of at least twenty specimens, and were calculated according the equation:

$$\sigma_f = \frac{3QL}{2lh^2} \quad (1)$$

where Q is the failure load, L is the span, l is the width and h is the height.

The Vickers hardness, H_V and fracture toughness, K_{IC}, were measured using a Vicker's diamond indenter (*Leco 100-A*, St. Joseph, MI) on surfaces polished down to 1 μm, with applied loads of 490 N. This load was chosen in order to obtain well-developed cracks (without chipping) emanating from the four corners of the indentation impression. The corresponding crack sizes were determined using an optical microscope (*Leica DMRM*, Cambridge, UK). The fracture toughness was calculated using the formula given by Miranzo and Moya.[16]

2.4. Wear test set-up and conditions

Wear test were performed by rubbing a MgO-partially stabilized ZrO_2 (MgO–PSZ) sphere 5 mm in diameter against the specimen surface in an oscillating friction machine (Model 77, Cameron-Plint, Wokinham, England, UK). The ZrO_2 spheres were held to avoid rolling during test. All tests were performed at room temperature with sliding speed of 0.15 m/s and 15 mm of total amplitude in the oscillating movement. At least four sliding wear tests were conducted from each composition. The weight loss was measured using an electronic balance (Mettler-Toledo, Swiss) with resolution of 0.01 mg, the specimen being removed periodically from the machine. Both the specimen and the sphere were cleaned ultrasonically in acetone prior to testing and every time the test was interrupted to determine the wear loss. The sliding distance of the tests was varied for each specific measurement to obtain significant wear. Normal loads of 20 up to 150 N were used. The corresponding initial Hertzian mean contact pressures, P, for normal loads were calculated from[17]:

$$P_{Hertz} = \frac{1}{3\pi}\left(\frac{3FE_r^2}{R_r^2}\right)^{1/3} \quad (2)$$

where F is the applied normal force; E_r, the reduced elastic modulus; and R_r, the reduced radius. E_r and R_r are defined by: $1/E = 1/2[(1-\nu_1{}^2)/E_1 + (1-\nu_2{}^2)/E_2]$ where E_1 and E_2 are the elastic moduli and ν_1 and ν_2 are Poisson's rations of sphere and material, respectively. $R_r = R/2$ where R is the radius of curvature of the sphere.

3. Results and discussion

Fig. 1 shows SEM images of a thermally etched, polished section of Al_2O_3–3Y-TZP composites. The ZrO_2 and Al_2O_3 grains are the brighter and darker phase, respectively. Mean grain size of alumina matrix for A22TZY, A14TZY and

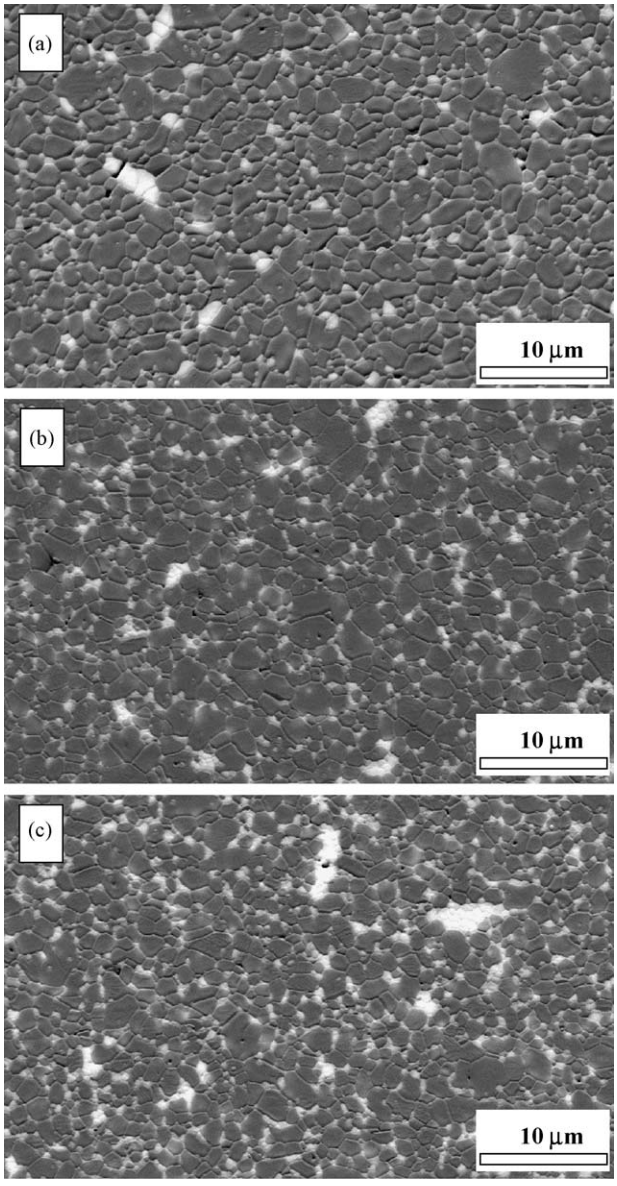

Fig. 1. SEM micrographs of (a) AL7TZY; (b) AL14TZY and (c) AL22TZY, after thermal etching, matrix grains are alumina, white grains are zirconia particles.

A7TZY composites were found to be: 2.0, 2.3 and 2.5 μm, respectively. The addition of zirconia along the grain boundaries is expected to lower the rate of alumina grain growth by grain pinning, so reducing the final alumina grain size. The magnitude of this effect is dependent on the amount of the zirconia grains present, with higher zirconia volume fractions resulting in a finer alumina grain size. In our composites

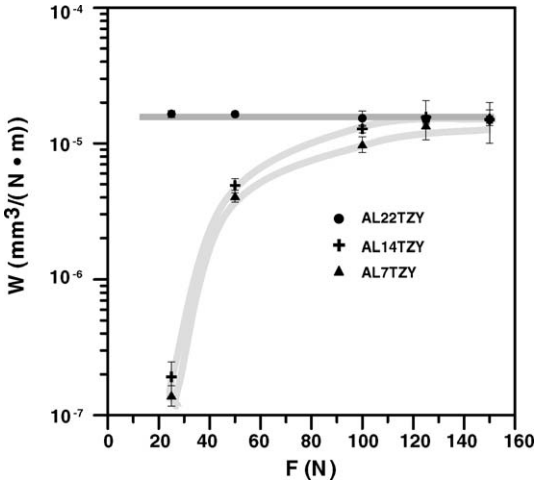

Fig. 2. Effect of normal loads on the wear rates of composite materials.

(from 7 to 22 vol.% 3Y-TZP) the alumina average grain size (2.0–2.5 μm) can be considered as a constant versus the wear test.

The strength, elastic modulus, Vickers hardness and toughness of the materials used for tribological tests are given in Table 1. It should be noted that the addition of 3Y-TZP increases the strength and fracture toughness of the composites, while the hardness and elastic modulus decreases, as expected according to the rule of mixtures.

The wear rate was computed as the volume loss divided by the sliding distance and the normal load.[18] This magnitude remained fairly constant in each test after a short transition period at the beginning, and the average values are plotted, in logarithmic scale, as a function of the contact load in Fig. 2.

SEM examination of the worn surfaces of the specimens reveals the difference in wear mechanisms. For AL7TZY ceramics, under a normal load of 20 N (Hertzian contact pressure of 1.1 GPa), a relatively smooth regions is observed (Fig. 3a). The small particle size of the wear debris indicated that they were probably removed from the material by plastic deformation and microcracking, these features are characteristic of abrasive wear. The plastic deformation of the materials is attributed to the large shear stress acting on the load zone. Fatigue processes due to repeated abrading on the top surface and the corresponding plastic deformation of the surface may result in microcracking. Wear debris adheres easily to the microcracked parts. Conversely, under normal load of 150 N (2.2 GPa) a rough region is observed (Fig. 3b). This region, which are very irregular and deeply grooved, indicates a large degree of microcracking at the contact surface and in the subsurface. The higher degree of microfractured regions results

Table 1
Mechanical properties of ATZ composites

	Stregth, σ_f (MPa)	Young modulus, E (GPa)	Toughness, K_{IC} (MPa m$^{1/2}$)	Hardness, H (GPa)
AL7TZY	517 ± 35	375	4.1 ± 0.2	16.7
AL14TZY	620 ± 65	360	4.5 ± 0.3	16
AL22TZY	760 ± 77	357	5.3 ± 0.3	15.9

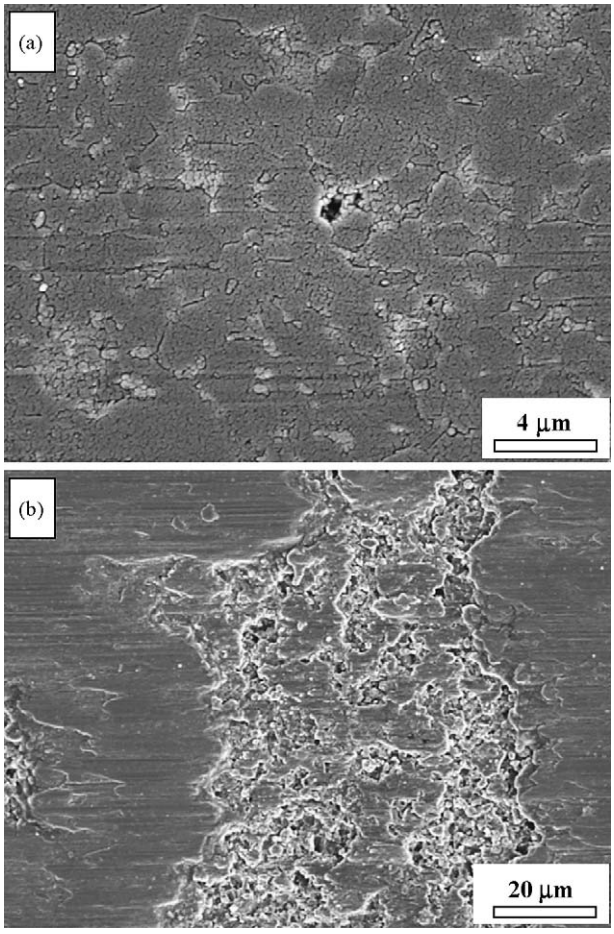

Fig. 3. SEM micrographs of the worn surface of AL7TZY composite after sliding against MgO–PSZ sphere under normal load of (a) 20 N and (b) 150 N.

in more wear debris adhering to the surface that deteriorates the material properties because the local contact stress is concentrated at the wear debris area and hence much larger. These high local stresses result in crack propagation near and/or beneath the wear debris regimes. This indicates that the wear mechanism is dominated by intergranular fracture and grain pull-out characteristic of chipping wear. Therefore, the transition from mild wear (plastic deformation controlled) to severe wear (microfracture controlled) has started at a normal load of 20 N. Removal of material by such different mechanisms led to different wear rates and worn surface roughness.

The zirconia transformation may be active during the wear process. The more tetragonal zirconia that transforms to monoclinic phase, the greater will be the stresses that are introduced. This stress induces phase transformation toughening at the crack tip and/or the formation of compressive stresses near the surface. This fact, may help the material resist crack propagation and hence reduce wear.[4,19] However, for a high normal loads ≥100 N (corresponding Hertzian contact pressure higher than 1.9 GPa), the increase of toughness in the composites with higher content of zirconia, is not enough to increase the resistance to wear. Therefore, the alumina matrix grain size is the main factor in characterizing the wear resistance of the composite materials at these loads, as has been determined previously for alumina materials.[20]

Pecharromán et al.[21] using IR reflectance measurements have stablished that the percolation threshold of alumina/3Y-TZP composites is located at 16 vol.% for 3-YTZP. In the case of compositions above this percolation threshold (AL22TZY), the wear rate at relatively low contact pressure of 20 N (1.1 GPa) was found to be around two orders of magnitude higher than the ones corresponding to 14 and 7 vol.% zirconia content, and very similar to the one obtained at higher loads (Fig. 2). The micrographs of the different Al_2O_3–3Y-TZP composites on the wear scar at low load (20 N) are show in Fig. 4. The wear path of AL22TZY shows a very irregular fracture and a rough surface, which is dominated by brittle fracture (Fig. 4c). Above the critical amount of ≈16 vol.% 3Y-TZP, geometrical percolation allows a continuous path between zirconia particles. The percolation phenomenon can be understood as a divergence in the inclusion size at the percolation threshold[22] or by a change in the topology of the minority phase, changing from isolated spheres to infinite cylinders.[23] Due to the complexity of systems at concentrations close to the percolation threshold, we have made a qualitative approach to determine the origin of the wear behaviour versus volume concentration.

Some authors have attributed the large wear rate values in pure 3Y-TZP[3,9,14] as a consequence of the thermal stresses induced by a gradient of temperature along the sample. In the case of Al_2O_3/3Y-TZP composites this model can not be applied due to the large thermal conductivity of the composite which is very close to that of alumina. It must be reminded that thermal conductivity of the composite brusquely changes when alumina concentration diminishes below its percolation concentration (around 16 vol.% of alumina, i.e. 84 vol.% of 3Y-TZP), but no appreciable changes in the effective thermal properties are observed in the range of concentrations from 0 to 50 3Y-TZP vol.%. Even more, the temperature gradient inside the 3Y-TZP particles can be determined by the expression:[24]

$$\nabla T(r,\theta) = \nabla T_0 \frac{\langle\kappa\rangle}{(1-L)\langle\kappa\rangle + L\kappa_z} \tag{3}$$

where $\langle\kappa\rangle$ is the effective thermal conductivity of the close environment of inclusion, which for low concentrations can be approximated by the alumina conductivity; κ_z, the zirconia conductivity; ∇T_0, the external temperature gradient and L which in the case of electric properties is called "depolarisation factor", here is assigned to be a shape coefficient. This expression is identical to that which determines the internal electric field inside an homogeneous matrix[23] because both thermal and electric properties are determined by the same Laplace equation and boundary conditions[25]:

$$\begin{aligned} \nabla(\sigma\nabla V) &= 0 \\ \nabla(\kappa\nabla T) &= 0 \end{aligned} \tag{4}$$

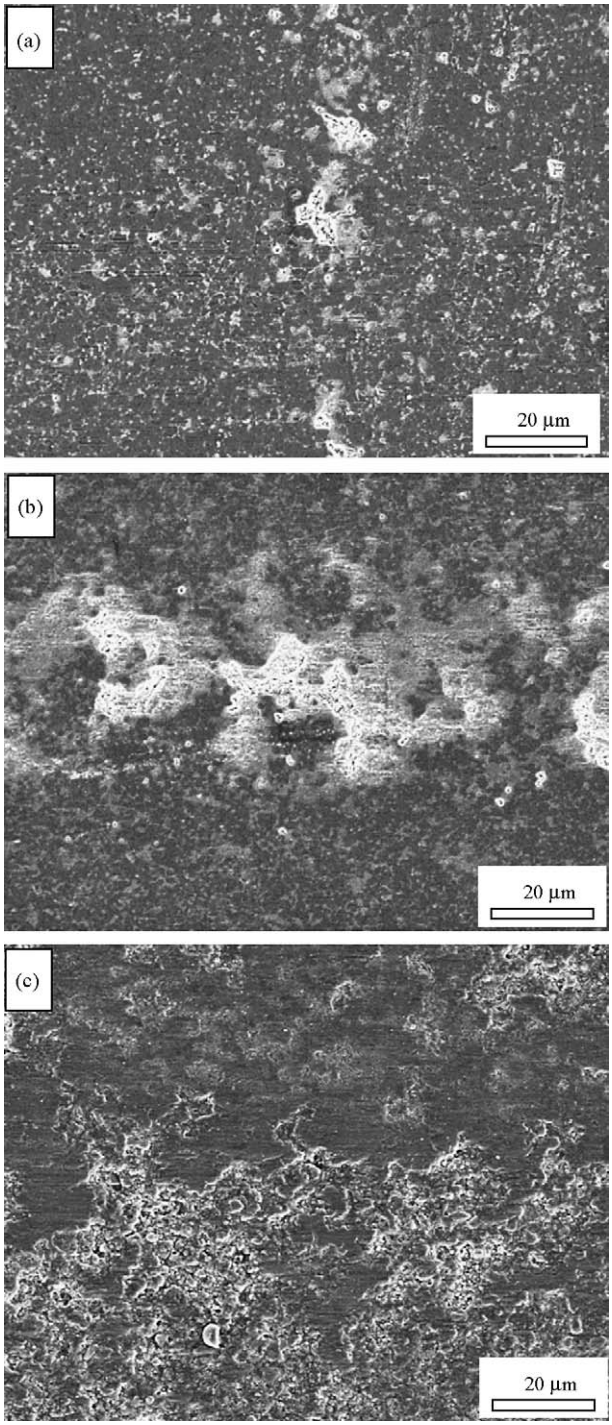

Fig. 4. SEM micrographs of the worn surface of (a) AL7TZY; (b) AL14TZY and (c) AL22TZY composites after sliding against MgO–PSZ sphere under normal load of 20 N.

where σ and V are the electric conductivity and potential, respectively. It should be noted that the internal field is determined by L, which is a crucial parameter in the spectral representation formalism.[22,23] This model, which has successfully explained the electric properties of many heterogeneous systems,[26] considers that an random heterogeneous system can be described by a distribution function of its shape parameter. In the case of low concentration, the distribution particle shape has a maximum at $L = 1/3$ corresponding to spherical inclusion, while according the concentration raises and exceeds the percolation threshold, it becomes a decreasing function with a maximum placed at $L = 0$, i.e. the shape coefficient of cylinders.[27] Experimental determination of spectral representation functions can be found in previous works.[28,29]

Thus we have just estimated the temperature gradients below and above the percolation threshold (f_c):

$$\nabla T(r,\theta) \approx \begin{cases} \nabla T_0 \dfrac{3\kappa_a}{2\kappa_a + \kappa_z} \approx \dfrac{3}{2}\nabla T_0 & \text{for } f < f_c \\ \nabla T_0 & \text{for } f > f_c \end{cases} \quad (5)$$

where f is the volume concentration of the 3Y-TZP particles and κ_a is the Al_2O_3 conductivity. We have used the approximation $\kappa_a \gg \kappa_z$. That is, the thermal gradient reduces a factor of 1.5 at percolation threshold. Because of thermal stresses are directly related with this magnitude, their value must reduce at percolation concentration comparing with low concentrations.

It is well known that thermal residual stresses arise during cooling from processing temperatures because of the thermal expansion mismatch between the zirconia particles ($\alpha_{zirconia} = 12 \times 10^6\,K^{-1}$) and the alumina matrix ($\alpha_{alumina} = 8.1 \times 10^6\,K^{-1}$). It is significant, however, that due to the homogeneous heating generated during wear test the magnitude of these stresses will be minimize. Thermal stresses for spheres (p_c) can be calculated by applying the Selsing formula[30] later modified by Fahmy and Ragai to take into account the inclusions volume concentration.[31] Following the same principle we have explicitly calculated the inner thermal stresses and the stress spatial distribution for cylinders.[32–34] In order to evaluate the effect of the geometrical change from spheres to cylinders on the mechanical properties, we have estimated a failure stress (Von-Mises stress) corresponding to both geometries as a function of volume concentration (Table 2).

$$\sigma_{VM} = \sqrt{\frac{1}{2}[(\sigma_1 - \sigma_2)^2 + (\sigma_2 - \sigma_3)^2 + (\sigma_3 - \sigma_1)^2]} \quad (6)$$

where σ_i ($i = 1, 2, 3$) are the main component of the stress tensor.

As we mentioned above, t → m zirconia phase transformation with ~4 vol.% increase, can be induced either thermally or by mechanical stresses (combination of both shear and tensile stress) during sliding. The zirconia phase transformation develops stresses of large magnitude which can be described by the same formalism as the conventional thermal stresses by substituting $\Delta\alpha\Delta T = \Delta V/3V$. As a result, in Fig. 5, we have plotted the failure criteria in the case of spherical and cylindrical zirconia inclusions transformation embedded into an alumina matrix. It must be reminded that for spherical inclusions, the internal stresses are isostatic so that the failure criterion is nil by definition.

Table 2
Stresses expressions originated in an homogenous solid composed by spheres of cylinders ideally embedded into a matrix

	Spheres	Cylinders
f	$\left(\frac{R_1}{R_2}\right)^3$	$\left(\frac{R_1}{R_2}\right)^2$
p_c	$\frac{\Delta\alpha\Delta T}{((1-2\nu_c)/E_c)+(1+\nu_s+2f(1-2\nu_s))/(2E_s(1-f))}$	$\frac{\Delta\alpha\Delta T}{((1-2\nu_c)(1+\nu_c)/E_c)+(1+\nu_s+f(1+\nu_s)(1-2\nu_s))/(E_s(1-f))}$
$(\sigma_{rr})_c$	p_c	p_c
$(\sigma_{\phi\phi})_c$	p_c	p_c
$(\sigma_{\theta\theta})_c$ $(\sigma_{zz})_c$	p_c	$-2\nu_c p_c$
$(\sigma_{VM})_c$	0	$(1+2\nu_c)p_c$
$(\sigma_{rr})_s$	$\frac{p_c}{1-f}\left[f-\left(\frac{R_1}{r}\right)^3\right]$	$\frac{p_c}{1-f}\left[f-\left(\frac{R_1}{r}\right)^2\right]$
$(\sigma_{\phi\phi})_s$	$\frac{p_c}{1-f}\left[f+\frac{1}{2}\left(\frac{R_1}{r}\right)^3\right]$	$\frac{p_c}{1-f}\left[f+\left(\frac{R_1}{r}\right)^2\right]$
$(\sigma_{\theta\theta})_s$ $(\sigma_{zz})_s$	$\frac{p_c}{1-f}\left[f+\frac{1}{2}\left(\frac{R_1}{r}\right)^3\right]$	$\frac{2\nu_s p_c f}{1-f}$
$(\sigma_{VM})_s$	$\frac{3}{2}\frac{p_c}{1-f}\left(\frac{R_1}{r}\right)^3$	$\frac{p_c}{1-f}\sqrt{3\left(\frac{R_1}{r}\right)^4+f^2(1-2\nu_s)^2}$

Subscript "*c*" refers to "core" or included particles and "*s*" to "shell" coating or matrix. R_1 refers to the particle radius, ZR_2 is the average distance between particles, E and ν are, respectively, the Young moduli and Poisson coefficients.

For low concentrations, 3Y-TZP appears as single particles embedded into an alumina matrix. So that, the combination of both homogeneous heating and the zirconia phase transformation has no effect on the particle failure criterion but large stresses will be introduced into the matrix. These localized stresses relax following a r^{-3} law (Table 2), and will increase monotonically with the 3Y-TZP concentration. As a result, in the case that an individual 3Y-TZP particle transforms, only a small shell around the particle will be mechanically affected being its thickness nearly concentration independent as it corresponds to the Von-Mises stress for spherical inclusions (Table 2).

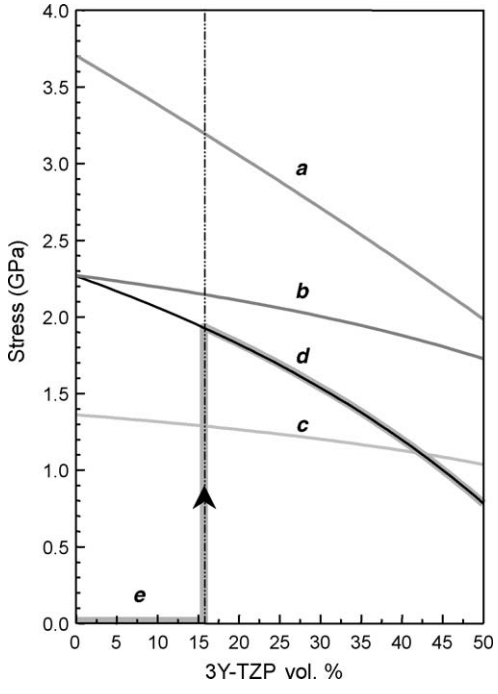

Fig. 5. Evolution of the stresses in the alumina matrix induced by 3Y-TZP martensitic transformation due to: (a) isostatic pressure of sphere, (b) radial and tangential component of cylinders and (c) longitudinal component of cylinders. Von-Mises stress at the interior of cylinders (d) and spheres (c). The dotted line represent the discontinuity from sphere to cylinders at percolation thershold (f_c).

However, once the percolation threshold is exceeded, long cylindrical zirconia clusters start to appear in the composite. In this case, large failure stresses can be found along the cylinders. These situation is the consequence of the development of radial (σ_{rr}) and angular expansive stresses ($\sigma_{\phi\phi}$, $\sigma_{\theta\theta}$) combined with tensile component along the longitudinal axis (σ_{zz}). Even more, the matrix induced stresses have a much larger range than in the case of spheres. In fact, they relax following a r^{-2} approximate law (Table 2). Additionally, these stresses increases nearly linearly versus volume concentration (f). As a result there is a dramatic change in the space failure stress distribution.

Finally, zirconia particles are no longer isolated for concentrations above the percolation threshold, so that once a single particle martensitically transforms, a long range fracture process will developed as observed in Fig. 4c corresponding to AL22YTZP composites.

4. Conclusions

- The wear rate at relatively low normal loads (20 N) for composition with zirconia content (22 vol.%) above the percolation threshold (16 vol.%) was up to two orders of magnitude higher than that of the composites below the percolation threshold (14 and 7 vol.%).
- The main wear mechanism for ZTA composites with zirconia content above the percolation threshold was identified as percolative mechanism that induced microcracking. Conversely, for ZTA composites with zirconia content below the percolation threshold, the main wear mechanisms were identified as abrasion at low loads (20 N) and chipping by inter- and transgranular cracking at higher loads ($\geq$100 N).

Acknowledgements

This work was supported by EU under project reference GRD2-2000-25039, by the Spanish Ministry of Science and Technology under projects number MAT2003-04199-C02 and MAT2003-05202-C02-02, and by the Comunidad de Madrid under project number GR/MAT/0357/2004. J.F.B. has been supported by Ministry of Science and Technology and CSIC under the "Ramón y Cajal" Program co-financed by European Social Fund.

References

1. Kerkwijk, B., Mulder, E. and Verweij, H., Zirconia–alumina ceramic composites with extremely high wear resistance. *Adv. Eng. Mater.*, 1999, **1**, 69–71.
2. Cherif, K., Gueroult, B. and Rigaud, M., Wear behaviour of alumina toughened zirconia materials. *Wear*, 1996, **199**, 113–121.
3. Kerkwijk, B., Winnubst, A. J. A., Verweij, H., Mulder, E. J., Metselarr, H. S. C. and Schipper, D. J., Tribological properties of nanoscale alumina–zirconia composites. *Wear*, 1999, **225–229**, 1293–1302.
4. Wang, Y. S., He, C., Hockey, B. J., Lacey, P. I. and Hsu, S. M., Wear transitions in monolithic alumina and zirconia–alumina composites. *Wear*, 1995, **181–183**, 156–164.
5. Sergo, V., Lughi, V., Pezzotti, G., Lucchini, E., Meriani, S., Muraki, N. *et al.*, The effect of wear on the tetragonal-to-monoclinic transformation and the residual stress distribution in zirconia-toughened alumina cutting tools. *Wear*, 1998, **214**, 264–270.
6. He, C., Wang, Y. S., Wallace, J. S. and Hsu, S. M., Effect of microstructure on the wear transition of zirconia-toughened alumina. *Wear*, 1993, **162–164**, 314–321.
7. Ravikiran, A., Subbanna, G. R. and Pramila Bai, B. N., Effect of interface layers formed during dry sliding of zirconia toughened alumina (ZTA) and monolithic alumina against steel. *Wear*, 1996, **192**, 56–65.
8. He, Y. J., Winnubst, A. J. A., Schipper, D. J., Burggraaf, A. J. and Verweij, H., Effects of a second phase on the tribological properties of Al_2O_3 and ZrO_2 ceramics. *Wear*, 1997, **210**, 178–187.
9. Metselaar, H. S. C., Kerwijk, B., Mulder, E. J., verweij, H. and Schipper, D. J., Wear of ceramics due to thermal stress: a thermal severity parameter. *Wear*, 2002, **249**, 962–970.
10. Thomsen, N. B. and Karihaloo, B. L., Optimum microstructure of transformation-toughened ceramics for enhanced wear performance. *J. Am. Ceram. Soc.*, 1995, **78**(1), 3–8.
11. Chen, Y. M., Rigaut, B. and Armanet, F., Wear behaviour of partially stabilized zirconia at high speed. *J. Eur. Ceram. Soc.*, 1990, **6**, 383–390.
12. Woydt, M., Kadoori, J., Habig, K.-H. and Hausner, H., Unlubricated sliding behaviour of various zirconia-based ceramics. *J. Eur. Ceram. Soc.*, 1991, **7**, 135–145.
13. He, Y., Winnubst, L., Burggraaf, A. J., Verweij, H., van der Varst, P. G. Th. and de With, B., Grain-size dependence of sliding wear in tetragonal zirconia polycrystals. *J. Am. Ceram. Soc.*, 1996, **79**, 3090–3096.
14. Lee, S. W., Hsu, S. M. and Shen, M. C., Ceramic wear maps: zirconia. *J. Am. Ceram. Soc.*, 1993, **76**, 1937–1947.
15. Mendelson, M. I., Average grain size in polycrystalline ceramic. *J. Am. Ceram. Soc.*, 1969, **52**, 443–446.
16. Miranzo, P. and Moya, J. S., Elastic/plastic indentation in ceramic: a fracture toughness determination meted. *Ceram. Int.*, 1984, **10**, 147–152.
17. http://www.tribology-abs.com.
18. Bhushan, B., *Modern Tribology Handbook, Vol 2, Materials, Coatings and Industrial Applications*. CRC, Florida, 2001, p. 1659.
19. He, Y. J., Winnubst, A. J. A., Burggraaf a., J., Verweij, H., van der Varst, P. G. T. and de With, G., Sliding wear of ZrO_2–Al_2O_3 composite ceramics. *J. Eur. Ceram. Soc.*, 1997, **17**, 1371–1380.
20. Cho, S.-J., Moon, H., Hockey, B. J. and Hsu, S. M., The trasition from mild to severe wear in alumina during sliding. *Acta Metall. Mater.*, 1992, **40**, 185–192.
21. Pecharromán, C., Bartolomé, J. F., Requena, J., Moya, J. S., Deville, S., Chevalier, J. *et al.*, Percolative mechanism of aging in zirconia-containing ceramics for medical applications. *Adv. Mater.*, 2003, **15**, 507–511.
22. Claro, F. and Fuchs, R., Optical-absorption by clusters of small metallic spheres. *Phys. Rev. B*, 1986, **33**, 7956–7960.
23. Bergman, D. J., Dielectric-constant of a composite-material-problem in classical. *Phys. Rep.*, 1978, **43**(9), 378–407.
24. Christensen, R. M., *Mechanism of Composite Materials*. Krieger Publishing Company, Florida, 1991.
25. Torquato, S., Random heterogeneous materials. *Microstructure and Macroscopic Properties*. Springer, New Jersey, 2001.
26. Stroud, D., Milton, G. W. and De, B. R., *Phys. Rev. B*, 1986, **34**, 5145–5153.
27. Poladian, L., *Phys. Rev. B*, 1991, **44**, 2092–2107.
28. Sturm, J., Grosse, P. and Theiss, W., *Zeit. Phys. B*, 1991, **83**, 361–365.
29. Day, A. R., Grant, A. R., Sievers, A. J. *et al.*, *Phys. Rev. Lett.*, 2000, **84**, 1978–1981.
30. Selsing, J., Internal stresses in ceramics. *J. Am. Ceram. Soc.*, 1961, **44**(8), 419.
31. Fahmy, A. A. and Ragai, A. N., Thermal-expansion behavior of 2-phase solids. *J. Appl. Phys.*, 1970, **41**, 5108.
32. Liu, D. M. and Winn, E. J., Microstresses in particulate-reinforced brittle composites. *J. Mater. Sci.*, 2001, **36**, 3487–3495.
33. Franklin, W. S., The problem of the stresses and strains in a long elastic hollow cylinder subjected to internal and external pressure, and to tension. *Phys. Rev.*, 1900, **11**, 176–180.
34. Landau, L. D. and Lifshitz, E. M., Course of theoretical physics, In *Elasticity Theory*, *Vol 7*, ed. S. A. Reverté (Spanish edition), Barcelona, 1969.